Publications of the Astronomical Society of the Pacific, 129:104202 (8pp), 2017 October https://doi.org/10.1088/1538-3873/aa7f25

Abundance Analyses of the New R Coronae Borealis Stars ASAS-RCB-8 and ASAS-RCB-10

B. P. Hema[1], Gajendra Pandey[1], Devika Kamath[2,3,4], N. Kameswara Rao[1,5], David Lambert[5], and Vincent M. Woolf[6]
[1] Indian Institute of Astrophysics, Bengaluru, Karnataka 560034, India; hema@iiap.res.in
[2] Department of Physics and Astronomy, Macquarie University, Sydney NSW 2109, Australia
[3] Australian Astronomical Observatory, P.O. Box 915, North Ryde, NSW 1670, Australia
[4] Instituut voor Sterrenkunde, KU Leuven, Celestignenlaan 200D bus 2401, B3001 Leuven, Belgium
[5] The W.J. McDonald Observatory, University of Texas, Austin, TX 78712-1083, USA
[6] Physics Department, University of Nebraska at Omaha, Omaha, NE 68182-0266, USA
Received 2017 June 2; accepted 2017 June 27; published 2017 August 24

Abstract

Abundance analyses of the two newly discovered R Coronae Borealis (RCB) stars ASAS-RCB-8 and ASAS-RCB-10 were conducted using high-resolution optical spectra and model atmospheres. Their chemical compositions place the pair among the majority class of RCBs. ASAS-RCB-10 is one of the most N-poor majority RCBs with an above average O abundance. Relative to ASAS-RCB-10, ASAS-RCB-8 is H poor by 1.6 dex, O-poor by 0.7 dex but N-rich by 0.8 dex suggesting a higher contamination by CNO-cycled material.

Key words: stars: abundances – stars: chemically peculiar – stars: distances

Online material: color figures

1. Introduction

R Coronae Borealis (RCB) stars are a rare class of yellow supergiants exhibiting very peculiar photometric and spectroscopic characteristics. RCB stars experience optical declines of up to several magnitudes at (presently) unpredictable times with return back to their maximum light after many days, months, or years. The dominant spectroscopic peculiarity is that their photospheres are hydrogen poor by about factors of thousands to millions of times. RCB stars are further divided into majority RCBs and minority RCBs (Lambert & Rao 1994). Most notably, the minority RCBs have much higher [Si/Fe] and [S/Fe] abundance ratios than the majority RCB stars.

Just over 100 RCB stars are known in the Galaxy, the Small Magellanic Cloud and the Large Magellanic Cloud. About 80 RCBs have been identified in the Galaxy according to Clayton (1996), Clayton et al. (2002, 2009), Hesselbach et al. (2003), Miller et al. (2012), Tisserand et al. (2008, 2013), Zaniewski et al. (2005). Of the known Galactic RCBs, abundance analyses are available for only about 15%, a small sample which may not be fully representative of the class. Unfortunately, some RCBs are cool with complex spectra dominated by molecular bands, principally C_2 and CN in the optical region, and, thus, are a severe challenge to quantitative spectroscopy and many others are too faint for high-resolution spectroscopy with present telescopes. In this paper, we provide chemical compositions for two recently discovered warm and relatively bright Galactic RCB stars.

The origin of RCB stars is not yet without mystery. The most likely scenario was proposed by Webbink (1984): a He-white dwarf merges with a CO-white dwarf to form the RCB with its bloated envelope around the C–O white dwarf. This scenario accounts at least qualitatively for the composition of the majority RCB stars including the striking discovery of high abundances of ^{18}O relative to ^{16}O in the cooler RCB stars and their likely relatives, the cool H-deficient carbon stars (Clayton et al. 2005, 2007; García-Hernández et al. 2009, 2010). Favorable discussions of observed and predicted surface compositions from a merger of a He with a C–O white dwarf are provided by Pandey & Lambert (2011), Jeffery et al. (2011) and Menon et al. (2013).

This paper aims to conduct an abundance analysis for two newly discovered Galactic RCB stars: ASAS-RCB-8 and ASAS-RCB-10, found by Tisserand et al. (2013). These and other RCB stars were discovered from photometry using the ASAS-3 ACVS1.1[7] variable star catalog. Low-resolution spectra were obtained to confirm that they were RCB stars.

Our abundance analysis also considers two other recently discovered RCB stars V532 Oph (Clayton et al. 2009) and V2552 Oph (Hesselbach et al. 2003; Kato & Katsumi 2003; Kazarovets et al. 2003). Abundance analyses of this pair have been previously reported: V2552 Oph by Rao & Lambert (2003) and V532 Oph by Kameswara Rao et al. (2014). New

[7] The ASAS-3 survey monitored the sky south of declination +28 deg between 2000 and 2010 to a limiting magnitude of $V = 14$.

Table 1
Log of the Observations for the Program Stars

Star	Date of Observation	V_{obs} (mag)	Obervatory	V_{rad} (km s^{-1})
V2552 Oph	22 May 2007	11	McDonald	63 ± 2
V2552 Oph	12 May 2014	11	La Palma	60 ± 2
ASAS-RCB-8	11 May 2014	11.2	La Palma	134 ± 2
ASAS-RCB-8	23 Sep 2012	10.9	McDonald	137 ± 1.5
ASAS-RCB-10	12 May 2014	11.4	La Palma	54 ± 1
V532 Oph[a]	13 May 2014	11.7	La Palma	5 ± 1

Note.
[a] V532 Oph's V_{rad} as determined by Kameswara Rao et al. (2014) is -4.6 ± 1.5 km s^{-1} and -2.7 ± 0.9 km s^{-1}, respectively, for two different epochs (see Table 1 of Kameswara Rao et al. 2014).

spectra of the pair are analyzed here, partly as a check on our analytical procedures.

2. Observations

High-resolution optical spectra of the program stars at their maximum light were obtained with the 1.2 m Mercator telescope at the Roque de Los Muchachos observatory, La Palma. The 1.2 m Mercator telescope is equipped with the high-resolution fiber-fed spectrograph, HERMES (High-efficiency and High-resolution Mercator Echelle Spectrograph) (Raskin et al. 2004). The spectra were acquired at a resolving power ($\lambda/d\lambda$) of 85000 over the whole wavelength domain from 3770 to 9000 Å. Before abundance analysis, application of smoothing increased the S/N ratio and lowered the resolving power to 35000 but the intrinsically broad stellar line profiles are barely affected. Spectra for the program stars, ASAS-RCB-8 and ASAS-RCB-10 were obtained along with spectra of V2552 Oph and V532 Oph. Spectrum of a rapidly rotating early-type star was also obtained for each set of observations along with other calibration spectra.

McDonald observatory spectra of ASAS-RCB-8 and V2552 Oph were obtained with the Robert G. Tull cross dispersed echelle spectrograph of the Harlan J. Smith 2.7 m reflector at the W. J. McDonald observatory (Tull et al. 1995). The spectral resolving power $R = \lambda/d\lambda$ was 40,000. The spectrum covers 3900–10000 Å with gaps beyond about 5600 Å where the echelle orders were incompletely captured on the Tektronix 2048 × 2048 CCD. (The McDonald spectrum of V2552 Oph differs from that analyzed by Rao & Lambert 2003.) Mercator and Tull spectra of the same object are well matched in strength and shape of spectral features.

The date of observation, the AAVSO visual-validated magnitude (V) at the time of observation and the helio-centric-corrected radial velocity are given in Table 1.

3. Interstellar Extinction and Absolute Magnitude

In this section, the interstellar reddening is estimated from the strengths of the diffuse interstellar bands (DIBs) and the distance from the radial velocities of the star and from interstellar Na D lines. Together the reddening and distance provide an estimate of a star's absolute magnitude and this magnitude with an estimate of the stellar mass defines a locus in the ($T_{\rm eff}$, $\log g$) plane which in conjunction with spectroscopic loci serves to constrain the atmospheric parameters $T_{\rm eff}$ and $\log g$.

DIBs are identified in the spectra of V532 Oph, V2552 Oph, ASAS-RCB-10 and ASAS-RCB-8. Equivalent widths of seven DIBs were measured. For estimating the reddening $E(B-V)$, we have used "equivalent width—reddening" relation given by Luna et al. (2008) and Herbig (1993). The estimated average $E(B-V)$ is 0.52, 0.76, 0.57 and 0.25 lead to A_V of 1.70, 2.39, 1.78 and 0.77 (assuming R of 3.1) for V2552 Oph, V532 Oph, ASAS-RCB-10 and ASAS-RCB-8, respectively. The A_V values are consistent with the estimates of Tisserand et al. (2013) of 1.89 and 0.62 for ASAS-RCB-10 and ASAS-RCB-8, respectively.

The near maximum light magnitudes for program stars are given in Table 1. V maximum values for the program stars were corrected for interstellar extinction. These extinction-corrected V_0 are, 9.3 ± 0.13 for V2552 Oph, 9.3 ± 0.15 for V532 Oph and 9.62 ± 0.15 for ASAS-RCB-10. AAVSO V band magnitudes that are available show a V magnitude for ASAS-RCB-8 of 10.91 ± 0.1. This V maximum value may then be corrected for interstellar extinction of 0.7 mag. resulting in V_0 of 10.2 ± 0.15. The estimates of $E(B-V)$ for V532 Oph are in excellent agreement with that of Kameswara Rao et al. (2014). But for V2552 Oph, our determinations of $E(B-V)$ are different from that of Rao & Lambert (2003).

Kinematics of the interstellar gas along the line of sight to ASAS-RCB-8 are revealed by the Na I D lines. As an aid to identifying the interstellar Na D components, we computed the expected radial velocity with respect to the local standard of rest (LSR) with distance in the direction of ASAS-RCB-8 using the model Galactic rotation given by Brand & Blitz (1993). Components with negative LSR radial velocities are not expected to occur in this direction. The Galactic rotation curve shows an almost linear increase of $V_{\rm lsr}$ with distance and suggests that the radial velocity of the star ($V_{\rm lsr} \sim 144$ km s^{-1}) might occur at a distance of 8 kpc. Presence of ISM clouds in front of a star provides a minimum distance to the star of 7 kpc and a lower limit to the absolute visual magnitude (M_V) of this star. The extinction-corrected V magnitude 10.2 ± 0.1 obtained earlier coupled with the distance estimate of 7 kpc provides the minimum M_V of -4.0 ± 0.2. However if the star is at a distance of 8 kpc the M_V would −4.3.

Similarly, the distance estimated for ASAS-RCB-10 is about 7.4 kpc for the star's LSR corrected radial velocity ($V_{\rm lsr}$) $\sim$ 66 km s^{-1}. Using the extinction-corrected V magnitude 9.62 $\pm$ 0.15 along with the distance estimate, the absolute magnitude of the star would be -4.7 ± 0.2. For V2552 Oph, the distance estimated is about 7.7 kpc for the star's LSR-corrected radial velocity ($V_{\rm lsr}$) $\sim$ 72 km s^{-1}. Using the extinction-corrected V magnitude 9.3 $\pm$ 0.13 along with the distance estimate, the absolute magnitude of the star would be -5.1 ± 0.2.

The bolometric correction for stars with the $T_{\rm eff}$ of 6750 K is expected to be small: $\sim$0.02 according to Flower (1996) for normal supergiants. Our adopted $M_{\rm bol}$ for the stars are -4.0 ± 0.2 for ASAS-RCB-8 and -4.7 ± 0.2 for ASAS-RCB-10 where the uncertainty includes an estimate arising from the uncertain distance determinations. Unfortunately, the distances can not yet be replaced by parallax-based estimates. Two of the four stars are in the presently available *GAIA* catalog (Gaia Collaboration 2016a, 2016b) but the parallaxes are quite uncertain: $\pi = 0.18 \pm 0.24$ mas for ASAS-RCB-10 and $\pi = 0.59 \pm 0.25$ mas for V2552 Oph.

As is well known, $M_{\rm bol}$ can be expressed in terms of effective temperature $T_{\rm eff}$, surface gravity $\log g$ and the stellar mass M as $M_{\rm bol} = M_{\rm bol,\odot} + 2.5 \log (g/g_{\odot}) - 10 \log (T_{\rm eff}/T_{\odot}) - 2.5 \log (M/M_{\odot})$.

A mass of $M/M_{\odot} = 0.7 \pm 0.2$ is assumed considering the proposed scenario for the origin of RCB stars (Weiss 1987; Iben et al. 1996). This relation for a given $M_{\rm bol}$ then provides a locus in the ($T_{\rm eff}$, $\log g$) plane which (see below) with other loci contributes to the determination of the atmospheric parameters $T_{\rm eff}$ and $\log g$.

4. Abundance Analysis

The abundance analysis is modeled closely on the analyses discussed in detail by Asplund et al. (2000) and followed in subsequent analyses by Rao & Lambert (2003) for V2552 Oph, Rao & Lambert (2008) for V CrA and Kameswara Rao et al. (2014) for V532 Oph. Lines selected for measurement were largely those chosen in these earlier studies with the exception that fluorine (F I) lines were chosen following Pandey et al. (2008) and the C_2 Swan bands were synthesized following Hema et al. (2012).

The local-thermodynamic equilibrium (LTE) line analyses of the program stars were conducted by combining the UPPSALA line-blanketed H-deficient model atmospheres constructed based on the usual assumptions: flux constant, plane-parallel layers in hydrostatic and LTE, with the UPPSALA equivalent width analysis program "EQWIDTH" (Asplund et al. 1997).

In the RCB stars, the chief source of continuum opacity in the optical spectra is photoionization of neutral carbon (Asplund et al. 2000). Hence, a line of element X is influenced by the abundance ratio X/C even though He is the most common species. Since carbon is the dominant opacity source, the observed C I lines from levels with excitation potentials similar to the levels providing the continuous opacity are insensitive to the stellar parameters. Indeed, the strength of a given C I line is expected to be of same strength in spectra of RCB stars of different stellar parameters, while the strength of the other elemental spectral lines will vary with the change in stellar parameters and the metallicity (Rao & Lambert 1996).

These expectations are confirmed but for one troubling surprise; the predicted strengths of C I lines are weaker than observed. Equivalently, the carbon abundance derived using the H-deficient line-blanketed model atmospheres is a factor of 4 or about 0.6 dex less than that adopted for the input model atmosphere. This discrepancy is dubbed the "carbon problem" by Asplund et al. (2000). Further insights into the carbon problem's resolution are potentially provided by observations of [C I] lines by Pandey et al. (2004) and the C_2 Swan bands (Hema et al. 2012). Asplund et al. (2000) proposed an array of resolutions with some now failing to satisfy constraints set by the [C I] and C_2 observations. Their favored resolution supposed that the photosphere of Nature's RCB stars exhibited a shallower temperature gradient than the photosphere emerging from a computer. In principle, this idea might also satisfy the [C I] and C_2 observations. As a temporary but probably adequate measure, Asplund et al. suggested that abundance ratios such as O/Fe might be little affected by the inability to resolve the carbon problem. Thus in what follows our focus is on abundance ratios. The abundance analysis is based on model atmospheres constructed for a C/He ratio of 1% by number, a value close to the mean of 0.6% for extreme helium stars (EHes) (see Table 1 of Jeffery et al. 2011). EHes are sufficiently hotter than RCB stars that helium provides the continuous opacity and, hence, the C/He ratio is measurable from the strengths of He and C lines. EHes and RCB stars are likely on very similar evolutionary tracks.

An appropriate model atmosphere from the Uppsala grid is selected using a series of indicators each providing a locus in the ($T_{\rm eff}$, $\log g$) plane. A measure of $T_{\rm eff}$ with only a slight dependence on $\log g$ is set by demanding excitation balance using permitted lines of Fe II, and permitted and forbidden lines of O I. The lower excitation potential for Fe II and O I lines range from 2.8 eV to 6.2 eV and 0 eV to 11 eV, respectively. Ionization balance set using lines of Fe I and Fe II, Mg I and Mg II, and Si I and Si II provided three loci. Finally, the locus corresponding to the $M_{\rm bol}$ estimate for a mass of $0.7 M_{\odot}$ provides the final locus. To conclude the selection of parameters, lines of C I, Fe I, N I, Ca I, S I and Si I were used for separate determinations of the microturbulence, a quantity essentially independent of effective temperature and surface gravity.

Since both V532 Oph and V2552 Oph have been analyzed previously, we compare our results with these previous estimates. Our determinations of the stellar parameters for the

Table 2
The Derived and the Previously Published Elemental Abundances for the RCB Stars V2552 Oph and V532 Oph

Elements	log$\epsilon(E)$ for V2552 Oph				log$\epsilon(E)$ for V532 Oph			
	Now[a]	n[a,b]	2003[c]	n[b,c]	Now[a]	n[a,b]	2014[d]	n[b,d]
H I	6.67	1	6.66	1	6.57	1	6.31	1
Li I	⋯	⋯	<0.96	1	⋯	⋯	<0.97	1
C I	9.0 ± 0.26	31	9.05 ± 0.24	17	8.82 ± 0.3	14	8.91 ± 0.34	14
N I	8.80 ± 0.3	17	8.96 ± 0.28	8	8.57 ± 0.23	10	8.57 ± 0.23	10
O I	8.0 ± 0.20	10	7.96 ± 0.21	6	8.03 ± 0.25	5	7.90 ± 0.34	6
Ne I	⋯	⋯	⋯	⋯	⋯	⋯	8.62 ± 0.21	3
F I	6.7 ± 0.04	4	⋯	⋯	6.55 ± 0.08	5	⋯	⋯
Na I	5.95 ± 0.28	3	6.14 ± 0.12	3	6.16 ± 0.13	4	6.22 ± 0.04	4
Mg I	6.8 ± 0.03	2	6.77 ± 0.09	2	6.8 ± 0.14	3	6.84 ± 0.10	3
Mg II	6.9	1	⋯	⋯	6.8	1	6.89	1
Al I	5.9 ± 0.18	5	5.78 ± 0.11	2	5.6 ± 0.23	4	5.81 ± 0.15	4
Al II	⋯	⋯	⋯	⋯	⋯	⋯	5.81 ± 0.15	4
Si I	6.74 ± 0.3	11	6.97 ± 0.22	5	6.95 ± 0.23	7	6.93 ± 0.21	7
Si II	7.0 ± 0.18	2	7.67 ± 0.28	2	6.82	1	6.82	1
S I	7.0 ± 0.24	8	6.77 ± 0.09	7	6.65 ± 0.27	7	6.76 ± 0.23	7
K I	⋯	⋯	4.48	1	4.73	1	4.83	1
Ca I	5.2 ± 0.3	13	5.34 ± 0.27	4	5.13 ± 0.23	6	5.19 ± 0.21	6
Sc II	2.8 ± 0.23	3	2.91 ± 0.23	3	2.57 ± 0.3	3	2.80 ± 0.27	3
Ti II	4.15 ± 0.20	3	4.11 ± 0.37	2	4.18 ± 0.12	2	4.21 ± 0.26	2
Fe I	6.50 ± 0.25	42	6.37 ± 0.27	21	6.44 ± 0.12	29	6.47 ± 0.21	31
Fe II	6.56 ± 0.2	10	6.42 ± 0.09	10	6.44 ± 0.12	10	6.51 ± 0.13	10
Ni I	5.63 ± 0.3	8	5.55 ± 0.18	5	5.57 ± 0.13	5	5.55 ± 0.13	5
Cu I	4.36 ± 0.02	2	3.95 ± 0.16	2	4.33 ± 0.08	2	4.08 ± 0.20	2
Zn I	⋯	⋯	4.31	1	⋯	⋯	4.41	1
Sr II	⋯	⋯	4.28	1	⋯	⋯	⋯	⋯
Y II	2.4 ± 0.15	5	2.29 ± 0.09	3	1.96 ± 0.06	5	2.08 ± 0.09	5
Zr II	2.5 ± 0.13	2	2.25±0.19	3	2.07 ± 0.08	3	2.11 ± 0.15	3
Ba II	0.8 ± 0.1	2	1.03 ± 0.09	3	⋯	⋯	1.45 ± 0.05	5
La II	⋯	⋯	0.63 ± 0.43	2	⋯	⋯	0.67 ± 0.30	2

Notes.
[a] Using the spectra from La Palma Observatory.
[b] n is the number of lines used in the analysis.
[c] from Rao & Lambert (2003).
[d] from Kameswara Rao et al. (2014).

V2552 Oph, for the spectra from McDonald and La Palma observatories are an excellent match and are in agreement with those adopted by Rao & Lambert (2003). From our analysis, the determined stellar parameters for V2552 Oph are, ($T_{\rm eff}$, log g, ξ_t): (6750 ± 250, 0.4 ± 0.5, 7.5 ± 1). Rao & Lambert (2003) adopted parameters (6750, 0.5, 7). Abundances for C/He = 1% models are compared in Table 2.

For V532 Oph, we compared the equivalent widths measured from the La Palma spectrum with those measured by Kameswara Rao et al. (2014) from their McDonald spectrum. Since these were an excellent match, we adopted the stellar parameters derived by Kameswara Rao et al. (2014). They are, ($T_{\rm eff}$ K, log g (cgs units), ξ_t km s^{-1}): (6750 ± 250, 0.5 ± 0.3, 7.5 ± 1.0).

The abundances from the previously published results and from this work are given in Table 2 for the program stars V2552 Oph and V532 Oph. The derived abundances in this study are in good agreement with that of the previously published results, except for minor differences in the abundances which are attributable to the errors in the measured equivalent widths and differences in the lines used. The consistency between our abundances and previously published results shows that our results for ASAS-RCB-8 and ASAS-RCB-10 will be on the scale established by Asplund et al. (2000).

The stellar parameters determined for the new RCB stars, ASAS-RCB-8 and ASAS-RCB-10 respectively are ($T_{\rm eff}$ K, log g (cgs units), ξ_t km s^{-1}): (6750 ± 250, 0.5 ± 0.5, 7 ± 1) and (6900 ± 250, 0.35 ± 0.5, 7 ± 1). Figures 1 and 2 show the log g versus $T_{\rm eff}$ plane for ASAS-RCB-8 and ASA-RCB-10, respectively. Adopted stellar parameters are indicated by a dot and error bars with the cross. Abundances are summarized in Table 3. The errors on elemental abundances given are the mean of line-to-line scatter of the abundances. The errors on the abundances due to the errors on the stellar parameters are

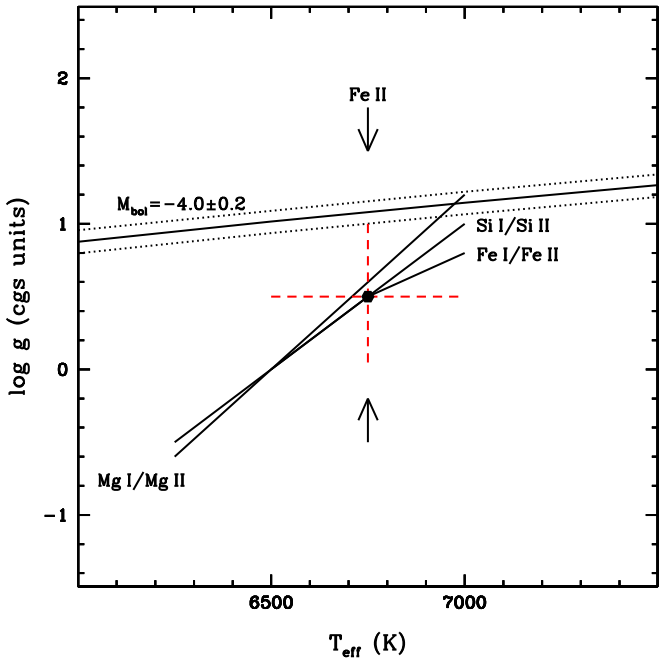

Figure 1. The log g vs. $T_{\rm eff}$ plane is shown for ASAS-RCB-8. Black up–down arrows mark the locus of the excitation balance for the Fe II lines. The loci of the ionization balance for the Mg I and Mg II, Si I and Si II, and Fe I and Fe II are shown. The locus for the determined $M_{\rm bol} = -4.0 \pm 0.2$ is also shown along with the loci for the errors on $M_{\rm bol}$ in dotted lines. The black dot and the red-dashed cross shows the final $T_{\rm eff}$–log g for the star.
(A color version of this figure is available in the online journal.)

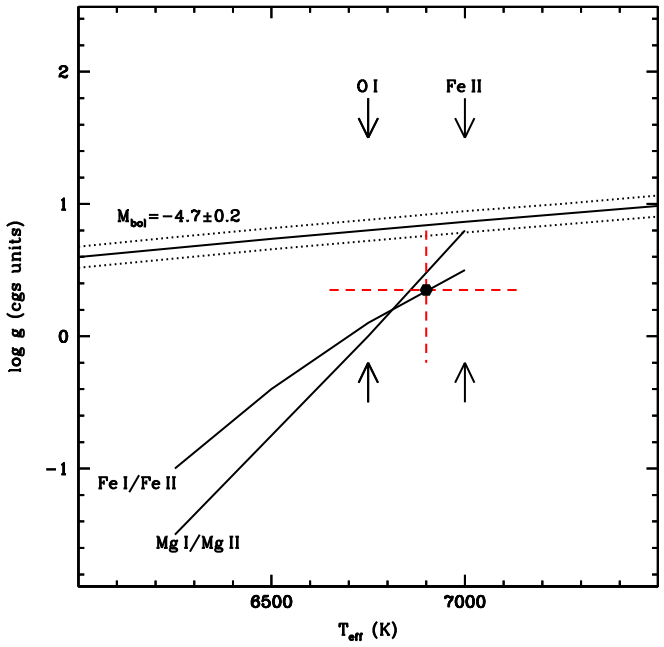

Figure 2. The log g vs. $T_{\rm eff}$ plane is shown for ASAS-RCB-10. Black up–down opposite arrows mark the loci of the excitation balance for the Fe II lines, and O I and [O I] lines. The loci of the ionization balance for the Mg I and Mg II and Fe I and Fe II are shown. The locus for the determined $M_{\rm bol} = -4.7 \pm 0.2$ is also shown along with the loci for the errors on $M_{\rm bol}$ in dotted lines. The black dot and the red-dashed cross shows the final $T_{\rm eff}$—log g for the star.
(A color version of this figure is available in the online journal.)

similar to those calculated by Asplund et al. (2000) (see Table 4 of Asplund et al. 2000). The effects of $\Delta\, T_{\rm eff}$, $\Delta \log g$, $\Delta\, \xi_t$ on the abundance ratios, (X/H) and (X/Fe) is less than 0.1 dex.

5. Chemical Composition

By all principal abundance indicators, ASAS-RCB-8 and ASA-RCB-10 belong to the majority class and not the minority class of RCB stars. Figure 3 (left-hand panel) shows abundance ratio [Si/Fe] versus [S/Fe] for RCB stars analyzed by Asplund et al. (2000) and others. Figure 3 (right-hand panel) shows these abundance ratios for EHe stars with data taken from (Jeffery et al. 2011 and the references therein).

ASAS-RCB-8 and ASAS-RCB-10 are positioned firmly in the majority clump, as are V532 Oph and V2552 Oph, as noted earlier by Rao & Lambert (2003) and Kameswara Rao et al. (2014). Certain minority RCB stars V3795 Sgr and V CrA are very cleanly separated from the majority stars. VZ Sgr also previously designated a minority RCB is less cleanly separated from majority RCBs. The spread in [Si/Fe] and [S/Fe] for RCBs and EHes appears to exceed the spreads expected from the abundance determinations. In previous discussions—for example, that by Rao & Lambert (2008)—DY Cen, which has been termed a hot RCB, appears as a minority RCB star. However, this appearance rested on a low Fe abundance (Jeffery & Heber 1993) but reanalysis by Pandey et al. (2014) including consideration of non-LTE effects places this hot RCB with the majority RCB stars. The EHe sample does not provide a minority star but they are spread out more than the RCB stars in [Si/Fe] and [S/Fe] along a line of a roughly constant Si/S ratio which is displaced about 0.4 dex from a similar line for the RCB stars.

The majority RCBs have similar but not identical compositions. In Figures 4 and 5 we show histograms for several elements with the pair of ASAS-RCB stars identified and minority RCBs distinguished from the majority stars. For the majority RCBs, the width of the histograms exceeds the likely errors with the largest widths occurring for H and Li (not shown). The 4 dex spread for H is obvious from the star-to-star differences in the appearance of the Hα line. Lithium is strongly present in a few stars and clearly absent in most including ASAS-RCB-8 and ASAS-RCB-10. For N and O, the histograms for majority RCBs spans about 1.5 dex. The Y abundances span about 2 dex. Inspection of Figure 5 shows that the Fe abundances are centered about the abundance 6.5 or a deficiency of 1 dex relative to the Sun. Given the carbon problem (see above), the Fe deficiency (and similar results for

Table 3
The Derived Elemental Abundances for the new RCB Stars ASAS-RCB-8 and ASAS-RCB-10

	ASAS-RCB-8[a]		ASAS-RCB-8[b]		ASAS-RCB-10[a]	
Elements	log$\epsilon(E)$	n[c]	log$\epsilon(E)$	n[c]	log$\epsilon(E)$	n[c]
H I	5.83	1	5.83	1	7.4	1
Li I	⋯	⋯	0.96	1	⋯	⋯
C I	9.0 ± 0.25	23	8.94 ± 0.27	13	9.1 ± 0.25	31
N I	8.58 ± 0.28	16	8.71 ± 0.29	11	7.8 ± 0.3	13
O I	8.09 ± 0.15	7	8.03 ± 0.26	7	8.66 ± 0.27	10
Ne I	⋯	⋯	8.53 ± 0.27	2	⋯	⋯
F I	6.87 ± 0.07	3	⋯	⋯	6.75 ± 0.15	4
Na I	6.35 ± 0.04	2	6.32 ± 0.05	3	5.92 ± 0.07	3
Mg I	6.79 ± 0.02	2	6.86 ± 0.75	4	6.83 ± 0.22	3
Mg II	6.71	1	6.51	1	6.7	1
Al I	6.1 ± 0.2	4	5.89 ± 0.17	5	5.6 ± 0.26	4
Al II	⋯	⋯	7.49	1	⋯	⋯
Si I	7.1 ± 0.27	10	7.5 ± 0.2	13	6.56 ± 0.27	10
Si II	7.15 ± 0.28	3	7.22 ± 0.4	3	7.0 ± 0.08	3
S I	7.08 ± 0.29	9	7.0 ± 0.14	8	6.65 ± 0.19	7
K I	4.93 ± 0.18	2	4.6 ± 0.3	2	4.68	1
Ca I	5.60 ± 0.3	13	5.45 ± 0.37	9	5.1 ± 0.28	12
Sc II	3.03 ± 0.3	4	2.74 ± 0.3	4	2.55 ± 0.24	3
Ti II	4.38 ± 0.26	3	4.29 ± 0.15	3	3.83 ± 0.25	3
Fe I	6.78 ± 0.20	37	6.57 ± 0.4	39	6.25 ± 0.27	38
Fe II	6.80 ± 0.13	15	6.46 ± 0.07	11	6.2 ± 0.29	12
Ni I	5.94 ± 0.17	7	5.69 ± 0.24	8	5.33 ± 0.30	3
Cu I	4.43 ± 0.23	2	4.11 ± 0.17	2	4.24 ± 0.25	2
Zn I	⋯	⋯	4.5	1	⋯	⋯
Sr II	⋯	⋯	2.28	1	⋯	⋯
Y II	2.33 ± 0.3	7	2.24 ± 0.14	5	1.5 ± 0.12	4
Zr II	2.56 ± 0.3	4	2.27 ± 0.14	3	2.1 ± 0.04	2
Ba II	1.5 ± 0.3	3	1.1 ± 0.2	3	0.80 ± 0.27	3
La II	⋯	⋯	0.89 ± 0.31	2	⋯	⋯

Notes.
[a] Using the spectra from LaPalma Observatory.
[b] Using the spectra from McDonald Observatory.
[c] n is the number of lines used in the analysis.

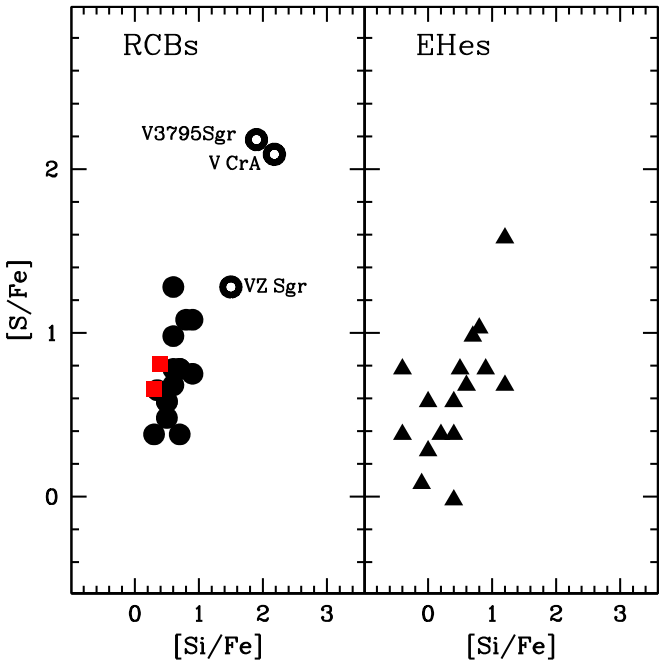

Figure 3. Abundance ratios of [Si/Fe] vs. [S/Fe] are given. The left panel shows the plot for RCB stars along with the two new RCBs ASAS-RCB-8 and ASAS-RCB-10 in red squares. The right panel shows the plot for EHes. (A color version of this figure is available in the online journal.)

other elements) may arise from use of an inappropriate atmospheric structure. However, the deficiency of Fe by about 1.0 dex relative to solar is roughly consistent with the "kinematic" abundance and supports the choice of C/He ratio of 1% for RCBs (for details see Rao & Lambert 1996). Insistence of the same C/He (=1.0% by number) across the sample may also have contributed to the spread in the histograms; for example, use of C/He =10% increases most abundances by 1.0 dex, i.e., would remove the Fe under-abundance. However, the adopted 1% C/He ratio is already almost a factor of two greater than the measured ratio for EHes stars, possible close relatives of the RCBs, as noted by Rao (2008).

Within the majority RCB population ASAS-RCB-10 has a low N and a high O abundance for a N/O ratio of −0.9 dex. ASAS-RCB-8 has the high N/O ratio of +0.6 dex. This reversal of the N/O ratio may indicate that ASAS-RCB-8 is now contaminated more severely than ASAS-RCB-10 with CNO-cycled H-burnt material. Consistent with this speculation is the lower H abundance of ASAS-RCB-8 and its generally higher metal abundance (the lower C abundance leads to lower continuous opacity and stronger metal lines, all being equal).

Spectra of all stars contain the C_2 Swan bands with and the (0, 0), (0, 1) and (1, 0) band heads at 5165, 5636 and 4737 Å, respectively. Spectrum synthesis was used to fit the observed bands—see Hema et al. (2012) for details. The derived carbon abundance from C_2 Swan bands for the new stars confirms the results of our previous study (Hema et al. 2012), that these derived abundances are independent of the adopted model atmosphere's carbon abundance. The derived carbon abundances from the (0, 1) C_2 band for V2552 Oph, V532 Oph, ASAS-RCB-8 and ASAS-RCB-10 are 8.1 ± 0.1, 8.2 ± 0.1, 8.3 ± 0.1, 8.2 ± 0.1, respectively, for C/He ratio 1%. The C abundance provided by the Swan bands and from C I lines is compromised by the lack of understanding of the carbon problem (see above). In principle, the (1, 0) band with the $^{12}C^{13}C$ head displaced to the red of the blue-degraded $^{12}C_2$ could provide an estimate of the $^{12}C/^{13}C$ ratio. Unfortunately, a Fe I line is blended with the $^{12}C^{13}C$ head. However, the $^{12}C^{13}C$ band head is almost reproduced by this Fe I line, indicating that there is very little or no ^{13}C present in these

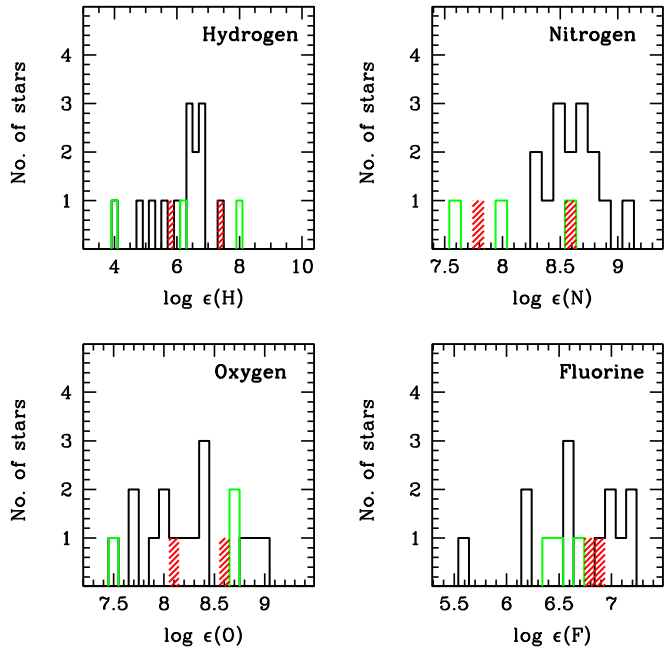

Figure 4. Frequency histograms of the elemental abundances for H, N, O and F are shown for the majority and minority and the two new RCB stars. Black line represents the majority RCB stars and green line the three minority RCB stars, and red hatched lines represent the new RCB stars ASAS-RCB-8 and ASAS-RCB-10.

(A color version of this figure is available in the online journal.)

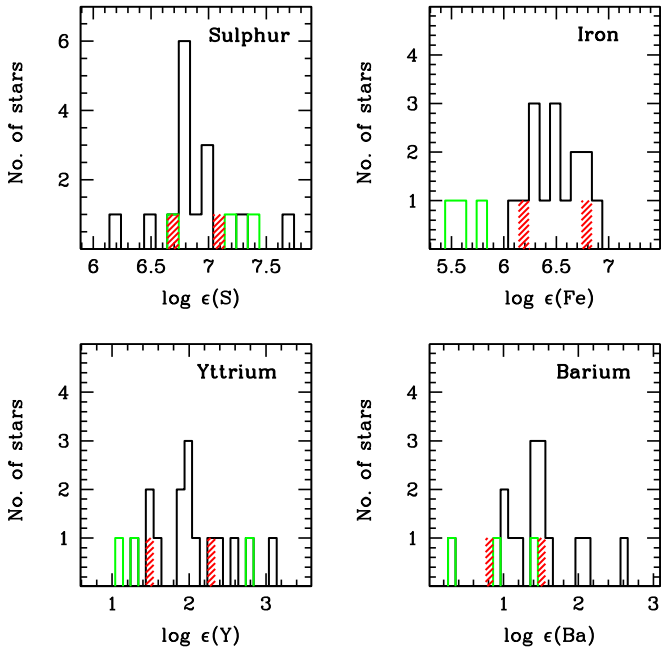

Figure 5. Frequency histograms of the elemental abundances of S, Fe Y, and Ba are shown for the majority and minority and the new RCB stars. Black line represents the majority RCB stars, green line represents the three minority RCB stars, and red hatched lines represent the new RCB stars ASAS-RCB-8 and ASAS-RCB-10.

(A color version of this figure is available in the online journal.)

stars. The high lower bound to the $^{12}C/^{13}C$ ratio is as expected for the merger product.

6. Circumstellar Dust

By chemical composition, ASAS-RCB-8 and ASAS-RCB-10 are representative of the majority class of RCB stars as defined by Lambert & Rao (1994). Within that class there is an apparent spread in composition including some real star-to-star differences. ASAS-RCB-8 and ASAS-RCB-10 are examples of these differences includng H, N and O.

Production of obscuring soot clouds with severe H-deficiency completes the pair of defining characteristics of RCB stars. Judged by their soot content, i.e., their infrared excess, the two new RCB stars are also representative of the majority class. The recent investigation of Spitzer spectra by Rao & Lambert (2015) explored the characteristics of the infrared excesses of RCB stars (García-Hernández et al. 2011, 2013). The spectral energy distribution (SED) for a star was constructed from optical and infrared photometry corrected for interstellar reddening. The SED was then fitted with a blackbody to represent the stellar flux and additional blackbodies to account for the circumstellar dust emission.

A SED for ASAS-RCB-8 was constructed for $E(B-V) = 0.23$ with optical photometry from AAVSO and near-infrared photometry from DENIS and 2MASS (quoted in Tisserand et al. 2013). Mid-infrared photometry is from the satellite *WISE* (Wright et al. 2010) in 2010. Blackbody fits to the stellar fluxes and the infrared emission by dust gives a stellar blackbody temperature of 7200 K and dust temperatures of 400 K. The fraction of stellar flux absorbed and reemitted by the dust is expressed by the covering factor $R = 0.005$ in 2010. This value of R is among the lowest values for RCB stars and probably not a surprise as Tisserand et al. (2013) remark "only one decline was observed during the ten year long ASAS-3 survey. With 0.003 mag day^{-1}, the decline rate is about 10 times slower than that of classical RCB stars."

Similarly for ASAS-RCB-10, blackbody fits for the stellar fluxes and the infrared emission by dust were made. Since the observed infrared fluxes from *WISE* and *AKARI* were different, separate fits were made. The derived dust temperatures are: 780 K and 730 K for *WISE* and *AKARI* observations, respectively. The infrared flux was lower at the time of *AKARI* observations relative to the *WISE* observations but the variability of the infrared flux is common among RCB stars. The R values for these observations are 0.20 from *WISE* and 0.13 from *AKARI*. The mean R value of 0.16 is taken for ASAS-RCB-10.

The amount of dust produced recently by the star (i.e., the factor R) was checked for correlation with the photospheric

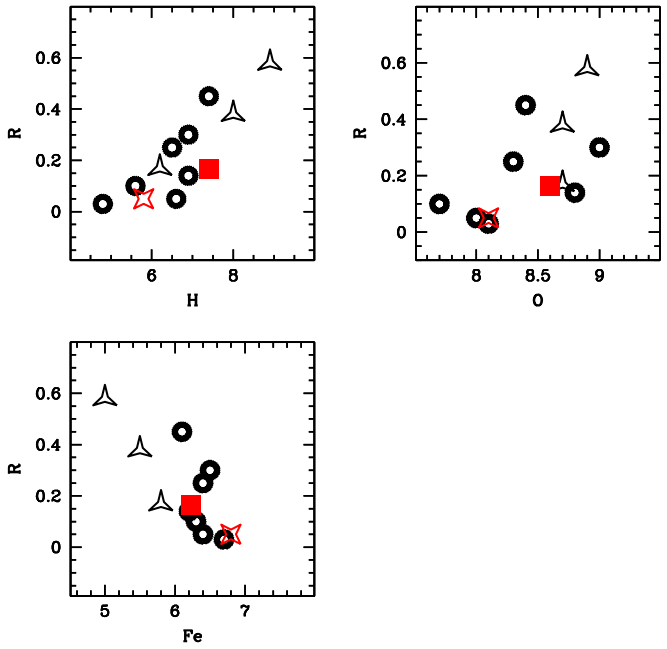

Figure 6. Dust covering factor R vs. the abundances of H, O, and Fe. The majority RCB stars are shown in black open circles, minority RCBs with open triangles, ASAS-RCB-8 with open red square and ASAS-RCB-10 with filled red square.

(A color version of this figure is available in the online journal.)

elemental abundances by Rao & Lambert (2015). The factor, R, indicating the amount of dust production shows correlation with the hydrogen, oxygen, and also carbon (Figures 6). R is anti-correlated with Fe (Figure 6). The new RCB stars ASAS-RCB-8 and ASAS-RCB-10 fall on the trends indicated by the previously known RCB stars and, in particular, anchor more firmly the low R end of the correlations.

7. Concluding Remarks

The RCB stars ASAS-RCB-8 and ASAS-RCB-10 are new additions to the group of majority RCBs having the elemental abundances similar to those of previously identified majority RCB stars. In addition, these new RCB stars support the correlations previously reported between stellar composition and the strength of the emission by the circumstellar dust.

D.L.L. acknowledges support from the Robert A Welch Foundation of Houston, Texas through grant F-634. N.K.R. would like to thank Satya and Vimala Mandapati for their kind hospitality during his stay in Austin. D.K. acknowledges the support of the KU Leuven contract GOA/13/012. D.K. acknowledges the support by the Fund for Scientific Research of Flanders grant G.OB86.13.

Based on observations obtained with the HERMES spectrograph, which is supported by the Research Foundation, Flanders (FWO), Belgium, the Research Council of KU Leuven, Belgium, the Fonds National de la Recherche Scientifique (FRS-FNRS), Belgium, the Royal Observatory of Belgium, the Observatoire de Geneve, Switzerland and the Thringer Landessternwarte Tautenburg, Germany.

References

Asplund, M., Gustafsson, B., Kiselman, D., & Eriksson, K. 1997, A&A, 318, 521
Asplund, M., Gustafsson, B., Lambert, D. L., & Rao, N. K. 2000, A&A, 353, 287
Brand, J., & Blitz, L. 1993, A&A, 275, 67
Clayton, G. C. 1996, PASP, 108, 225
Clayton, G. C., Geballe, T. R., Herwig, F., Fryer, C., & Asplund, M. 2007, ApJ, 662, 1220
Clayton, G. C., Hammond, D., Lawless, J., et al. 2002, PASP, 114, 846
Clayton, G. C., Herwig, F., Geballe, T. R., et al. 2005, ApJL, 623, L141
Clayton, G. C., Kilkenny, D., Wils, P., & Welch, D. L. 2009, PASP, 121, 461
Flower, P. J. 1996, ApJ, 469, 355
Gaia Collaboration, Brown, A. G. A., Vallenari, A., Prusti, T., et al. 2016a, A&A, 595, A2
Gaia Collaboration, Prusti, T., de Bruijne, J. H. J., Brown, A. G. A., et al. 2016b, A&A, 595, A1
García-Hernández, D. A., Hinkle, K. H., Lambert, D. L., & Eriksson, K. 2009, ApJ, 696, 1733
García-Hernández, D. A., Lambert, D. L., Kameswara Rao, N., Hinkle, K. H., & Eriksson, K. 2010, ApJ, 714, 144
García-Hernández, D. A., Rao, N. K., & Lambert, D. L. 2011, ApJ, 739, 37
García-Hernández, D. A., Rao, N. K., & Lambert, D. L. 2013, ApJ, 773, 107
Hema, B. P., Pandey, G., & Lambert, D. L. 2012, ApJ, 747, 102
Herbig, G. H. 1993, ApJ, 407, 142
Hesselbach, E., Clayton, G. C., & Smith, P. S. 2003, PASP, 115, 1301
Iben, I., Jr., Tutukov, A. V., & Yungelson, L. R. 1996, ApJ, 456, 750
Jeffery, C. S., & Heber, U. 1993, A&A, 270, 167
Jeffery, C. S., Karakas, A. I., & Saio, H. 2011, MNRAS, 414, 3599
Kameswara Rao, N., Lambert, D. L., Woolf, V. M., & Hema, B. P. 2014, PASP, 126, 813
Kato, T., & Katsumi, H. 2003, IBVS, 5417, 1K
Kazarovets, E. V., Kireeva, N. N., Samus, N. N., & Durlevich, O. V. 2003, IBVS, 5422, 1K
Lambert, D. L., & Rao, N. K. 1994, JApA, 15, 47
Luna, R., Cox, N. L. J., Satorre, M. A., García Hernández, D. A., et al. 2008, A&A, 480, 133
Menon, A., Herwig, F., Denissenkov, P. A., et al. 2013, ApJ, 772, 59
Miller, A. A., Richards, J. W., Bloom, J. S., et al. 2012, ApJ, 755, 98
Pandey, G., Kameswara Rao, N., Jeffery, C. S., & Lambert, D. L. 2014, ApJ, 793, 76
Pandey, G., & Lambert, D. L. 2011, ApJ, 727, 122
Pandey, G., Lambert, D. L., Rao, N. K., et al. 2004, MNRAS, 353, 143
Pandey, G., Lambert, D. L., & Rao, N. K. 2008, ApJ, 674, 1068
Rao, N. K. 2008, in ASP Confe. Ser. 391, Hydrogen-Deficient Stars, ed. A. Werner & T. Rauch (San Francisco, CA: ASP), 25
Rao, N. K., & Lambert, D. L. 1996, in ASP Conf. Ser. 96, Hydrogen Deficient Stars, ed. C. S. Jeffery & U. Heber (San Francisco, CA: ASP), 43
Rao, N. K., & Lambert, D. L. 2003, PASP, 115, 1304
Rao, N. K., & Lambert, D. L. 2008, MNRAS, 384, 477
Rao, N. K., & Lambert, D. L. 2015, MNRAS, 447, 3664
Raskin, G., Van Winckel, H., & Davignon, G. 2004, Proc. SPIE, 5492, 322
Tisserand, P., Clayton, G. C., Welch, D. L., et al. 2013, A&A, 551, A77
Tisserand, P., Marquette, J. B., Wood, P. R., et al. 2008, A&A, 481, 673
Tull, R. G., MacQueen, P. J., Sneden, C., & Lambert, D. L. 1995, PASP, 107, 251
Webbink, R. F. 1984, ApJ, 277, 355
Weiss, A. 1987, A&A, 185, 178
Wright, E. L., Eisenhardt, P. R. M., Mainzer, A. K., et al. 2010, AJ, 140, 1868
Zaniewski, A., Clayton, G. C., Welch, D. L., et al. 2005, AJ, 130, 2293